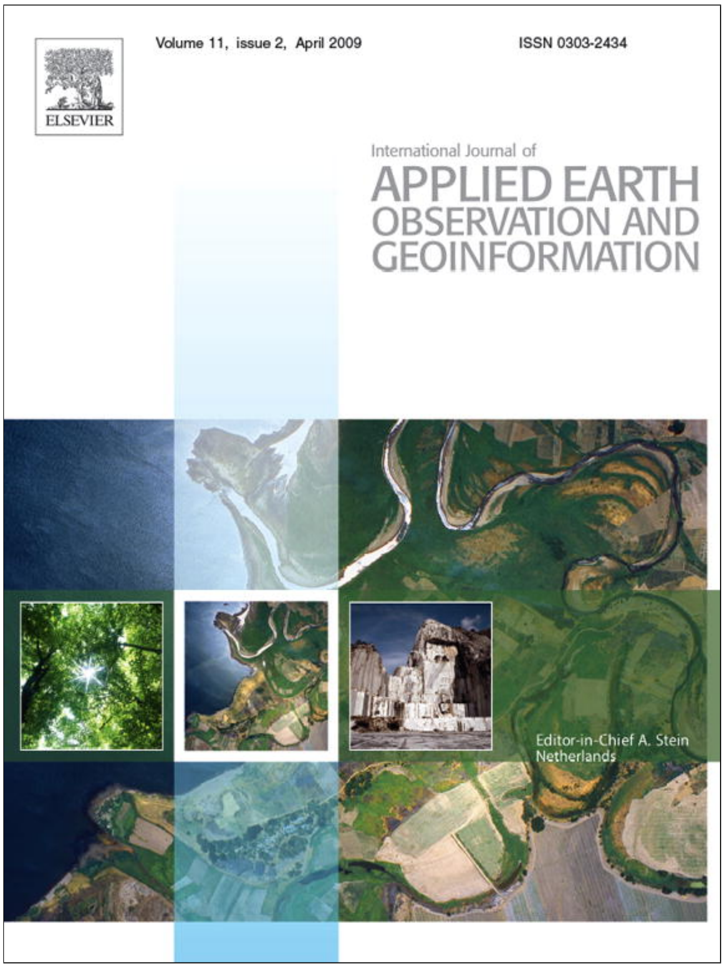
Volume 11, issue 2, April 2009
ISSN 0303-2434
ELSEVIER
International Journal of
APPLIED EARTH
OBSERVATION AND
GEOINFORMATION
Editor-in-Chief A. Stein
Netherlands

International Journal of Applied Earth Observation and Geoinformation 11 (2009) 114–129

Contents lists available at ScienceDirect

International Journal of Applied Earth Observation and Geoinformation

journal homepage: www.elsevier.com/locate/jag

A global map of rainfed cropland areas (GMRCA) at the end of last millennium using remote sensing

Chandrashekhar M. Biradar [a,*], Prasad S. Thenkabail [b], Praveen Noojipady [c], Yuanjie Li [c], Venkateswarlu Dheeravath [d], Hugh Turral [e], Manohar Velpuri [f], Murali K. Gumma [b], Obi Reddy P. Gangalakunta [g], Xueliang L. Cai [h], Xiangming Xiao [a], Mitchell A. Schull [i], Ranjith D. Alankara [d], Sarath Gunasinghe [d], Sadir Mohideen [d]

[a] Center for Spatial Analysis, University of Oklahoma, Norman, OK, USA
[b] U.S. Geological Survey (USGS), Flagstaff, Arizona, USA. Formerly, IWMI, Colombo, Sri Lanka
[c] Department of Geography, University of Maryland, College Park, MD, USA
[d] International Water Management Institute, Colombo, Sri Lanka
[e] On the Street Productions, North Carlton, Melbourne 3054, Australia
[f] GIS Center of Excellence, South Dakota State University, Brookings, SD, USA
[g] National Bureau of Soil Survey and Land Use Planning, Indian Council for Agricultural Research, India
[h] College of Water Resources and Hydropower, Wuhan University, Wuhan, China
[i] Department of Geography and Environment, Boston University, Boston, MA, USA

ARTICLE INFO

Article history:
Received 7 February 2008
Accepted 20 November 2008

Keywords:
Global mapping
GMRCA
Rainfed and irrigated croplands
Remote sensing
Sub-pixel areas

ABSTRACT

The overarching goal of this study was to produce a global map of rainfed cropland areas (GMRCA) and calculate country-by-country rainfed area statistics using remote sensing data. A suite of spatial datasets, methods and protocols for mapping GMRCA were described. These consist of: (a) data fusion and composition of multi-resolution time-series mega-file data-cube (MFDC), (b) image segmentation based on precipitation, temperature, and elevation zones, (c) spectral correlation similarity (SCS), (d) protocols for class identification and labeling through uses of SCS R^2-values, bi-spectral plots, space-time spiral curves (ST-SCs), rich source of field-plot data, and zoom-in-views of Google Earth (GE), and (e) techniques for resolving mixed classes by decision tree algorithms, and spatial modeling. The outcome was a 9-class GMRCA from which country-by-country rainfed area statistics were computed for the end of the last millennium. The global rainfed cropland area estimate from the GMRCA 9-class map was 1.13 billion hectares (Bha). The total global cropland areas (rainfed plus irrigated) was 1.53 Bha which was close to national statistics compiled by FAOSTAT (1.51 Bha). The accuracies and errors of GMRCA were assessed using field-plot and Google Earth data points. The accuracy varied between 92 and 98% with kappa value of about 0.76, errors of omission of 2–8%, and the errors of commission of 19–36%.

1. Introduction

The importance of rainfed croplands cannot be over-emphasized. Rainfed croplands meet about 60% of the food and nutritional needs of the World's population and are backbone of the marginal or subsistence farmers. They are increasingly seen as better alternative to irrigated agriculture as a result of its environmental friendliness and sustainability over long periods of time. Roughly 80% of the agricultural land worldwide is under rainfed agriculture, with generally low yield levels and high on-farm water losses (Rockstrom et al., 2003). This suggests a significant window of opportunity for improvements. The ballooning population is putting enormous strain on freshwater resources, and it has become increasingly clear that the challenge of feeding tomorrow's world population is, to a large extent, about improved water productivity within present land use; specifically in rainfed cropland areas (CA, 2007). The theoretical potential for cropland areas in the present climatic conditions and based on soil, climate, and topography are estimated at 3.29 billion hectares or Bha (Xiao et al., 1997) to 4.15 Bha (Cramer and Soloman, 1993). However, it must be noted that the productivity of a large proportion of these lands is limited due to poor soil fertility, soil depth, access to water,

* Corresponding author at: Center for Spatial Analysis, Stephenson Research and Technology Center, 101 David L. Boren Blvd, Norman, OK 73019, USA.
Tel.: +1 405 325 5568; fax: +1 405 325 3442.
E-mail addresses: chandra.biradar@ou.edu, c.biradar@gmail.com (C.M. Biradar), pthenkabail@usgs.gov, thenkabail@gmail.com (P.S. Thenkabail).

0303-2434/$ – see front matter © 2008 Elsevier B.V. All rights reserved.
doi:10.1016/j.jag.2008.11.002

and disease (e.g., Tse-tse flies and the black fleas). Land conversions from forests, rangelands, protected areas will be environmentally costly (Richards, 1990) and ecologically unacceptable. Thereby, any increase will have to come from increased productivity and/or intensification of rainfed croplands. In addition, rainfed agriculture is generally known to be far better sustainable than irrigated agriculture which is, often, associated with water logging and soil salinisation. The rainfed cropland has a history of roughly 10,000 years compared to about 6000 years history of irrigated agriculture (World Resources, 1992–1999; Mackenzie and Mackenzie, 1995).

Literature shows that the World's cropland estimates vary from 1.11 to 3.62 Bha (Hansen et al., 2000; FAOSTAT, 2000; WRI, 2000; Loveland et al., 2000; Goldewijk, 2001). It is well known that no two global datasets match (Defries and Townshend, 1994) as a result of differences in definitions, methods, data sources, data types, data calibration, and data acquisition modes. Cropland area increase has been only modest from 1.36 Bha in 1960 to 1.47 Bha in 1990. Based on various estimates, it has remained around 1.5–1.8 Bha at the end of the millennium (Ramankutty and Foley, 1999; World Resources, 1992–1999), of which about 16–18% is irrigated (Siebert et al., 2006; Thenkabail et al., 2008). However, the above efforts do not differentiate between the rainfed and irrigated croplands.

Past global maps were focused on land use/land cover (LULC) while not specifically concentrating on rainfed or irrigated croplands. The commonly used global LULC datasets were primarily non-remote sensing based, produced using data from various maps at 100-km grid by Matthews (1983), and 50-km grid by Olson and Watts (1982), Olson (1994), and Wilson and Henderson-Sellers (1985). More recently, AVHRR and MODIS sensor data have been widely used to produce global LULC. The 1992–1993 AVHRR 1-km data were used by USGS (Loveland et al., 1999, 2000) and University of Maryland (Defries et al., 1995, 1998) to produce global LULC datasets. These data also were used by IGBP (Loveland et al., 2000). The most recent LULC products are from Boston University using MODIS (Friedl et al., 2002) and GLC2000 using Spot Vegetation data (Bartholomé and Belward, 2005).

The spatial distribution of cropland areas are also changing. For example, in certain regions cropland areas are shrinking in recent times as a result of soil degradation, urbanization, and desertification and global warming. Between the early 1960s and the late 1990s, world cropland grew by only 11%, while world population almost doubled. As a result, cropland per person fell by 40%, from 0.43 ha to only 0.26 ha (FAO, 2002). In the future, 80% of increased crop production in developing countries will have to come from intensification: higher yields, increased multiple cropping, and shorter fallow periods. At the same time, cropland areas are increasing in certain parts of the world such as the African and Amazonian rainforests where slash-and-burn agriculture expansion with decreasing fallow periods and expansion for bio-fuel cultivation are major factors. In addition, changes are occurring in cropping pattern (e.g., vegetables in place of grains) and intensification (e.g., double crop in place single crop).

Therefore, there is a clear need to determine precise extent of rainfed cropland areas and their spatial distribution. Given this importance, the present research has been carried out to produce the first satellite sensor based global map of rainfed cropland areas (GMRCA) using: (a) monthly time-series pathfinder AVHRR 10-km data for 1999–2001, (b) SPOT VGT monthly 1-km data for 1999, and (c) a suite of secondary data. The objectives of this research were to: (a) develop methods and produce a global map of rainfed cropland areas using remote sensing and secondary data, (b) calculate rainfed cropland areas for every country in the world, and (c) establish accuracies and errors of such an estimate.

2. Datasets

2.1. Satellite data and ancillary data

The satellite sensor and ancillary data, with global coverage, used in this research consisted of: (a) NOAA AVHRR 10-km monthly data for 1997–1999, (b) SPOT VGT 1-km monthly data for 1999, (c) GTOPO30 1-km digital elevation data, (d) University of East Anglia Climate Research Unit's (CRU's) 50-km precipitation monthly data for 1961–2001, (e) skin temperature data derived from NOAA AVHRR for 1997–1999, (f) Google Earth (GE) very high resolution imagery (VHRI) "zoom-in-views" of over 15,000 points, and (g) field-plot data points from nearly 8000 points sourced from degree confluence project (DCP) and collected during this research. The detail descriptions of the above data sets are explained in the Thenkabail et al. (2006, 2008).

2.2. Mega-file data-cube (MFDC) of time-series satellite sensor data

Most of the global agricultural land use types are seasonal in nature in terms of the canopy cover, growth, and senescence of vegetation strata. Mapping and monitoring agricultural seasonality at the global level requires information at high temporal frequency. Remote sensing data allows us to obtain such time responsive information at a global scale (IGBP, 1992). In this study, we use state-of-art pathfinder time-series satellite data derived from NOAA AVHRR (http://www.iwmidsp.org), SPOT-Vegetation (http://www.spot-vegetation.com), and a suite of secondary data (Table 1) to map the rainfed croplands of the world. Time-series data helps to differentiate the dynamics of agriculture to delineate rainfed croplands from other LULC types. Table 1 describes the dataset used and its characteristics. Arrangement of datasets was one of the important components for the time-series analysis. Time-series data sets were arranged as layer by layer (layer stack) in common projection and uniform unsigned 8-bit level to synchronize the variability from its original form to generate a single mega-file data-cube of 159 layers in image processing software (e.g., ER-Mapper and ERDAS Imagine) consisting of data outlined with characteristics in Table 1. This single MFDC was resampled and saved as 1-km grid file, the volume of which was 110GB. This consisted of (Table 1): (a) 144 AVHRR layers from 3 years (12 layers with 1 layer per month $\times$ 4 bands per month with red, near-infrared, thermal infrared, and NDVI layers, $\times$3 years), (b) 12 SPOT layers from 1 year, (c) a single layer of elevation, (d) a single layer of mean rainfall for 40 years, and (d) a single layer of forest cover (Table 1). Table 1 describes the dataset used and its characteristics.

2.3. Field-plot data

Field-plot data is important to understand the real situation on the ground for class identification, naming, and accuracy assessment. One of the strengths of this work is the collection of a large volume of field-plot data (Fig. 1) that is made available to public through International Water Management Institute's Data Storehouse Pathway (IWMIDSP; http://www.iwmidsp.org). The three distinct field-plot data are described below.

2.3.1. GMRCA project field-plot data

A total of 1861 field-plot points were collected during various field campaigns in India, China, Central Asia, West Africa, Middle East, and Southern Africa. The data consist of precise location, land use/land cover, irrigated croplands, rainfed croplands, canopy cover percentage, and digital photos. Of this 936 points were used during the class identification and labeling and the remaining 915 were reserved for class accuracy assessment of GMRCA.

Table 1
Mega-file data characteristics. A single global mega-file of 159 bands was composed by fusing AVHRR 10-km, SPOT VGT 1-km, and a suite of secondary data. All data were re-sampled to 1-km in the mega-file.

Band number or primary source (#)	Wavelength range (μm)	Duration (year)	Number of bands and radiometry (#; one per month)	Data final format *Z*-scale (percent: for reflectance)	Range
Satellite sensor data					
AVHRR 10-km					
Band 1 (B1)	0.58–0.68	1997–1999	36	Reflectance @ ground, 8-bit	0–100
Band 2 (B2)	0.73–1.1	1997–1999	36	Reflectance @ ground, 8-bit	0–100
Band 4 (B4)	10.3–11.3	1997–1999	36	Brightness temperature	160–340
(Top-of-atmosphere) NDVI	(B2 − B1)/(B2 + B1)	1997–1999	36	Unitless, 8-bit scaled NDVI	−1 to +1
SPOT VGT 1-km					
NDVI	(B2 − B1)/(B2 + B1)	2000	12	Unitless, 8-bit scaled NDVI	−1 to +1
Secondary data					
GTOPO30 1-km					
One-band	DCW, DTM, and others	1 time	1	Meters, 16-bit	−1 to +1
Rainfall 1-km					
One-band	Mean of monthly 40-years	1961–2001	1	mm, 16-bit	0–65536
Forest cover 1-km					
One-band	None	1992–1993	1	Class names, 8-bit	0–256

2.3.2. Google Earth field-plot (GE-FP) data

A total of 11,000 locations of sub-meter to 0.6–4 m very high resolution imagery zoom-in-views from Google Earth were used as "field-plot areas". These areas of interests (AOIs) provided visual information on various landscape feature and classes such as agriculture, forests, barren, and existence of irrigation structure (e.g., canals, tanks and reservoirs). The visual interpretation keys such as such as shape, size, texture, pattern, tone, and association were used to distinguish the various LULC classes (Lillesand and Kiefer, 1987) Using Google Earth very high resolution images as AOIs have an advantage over point based field-plot in that it provides information on much larger areas, and therefore more representative view than is normally sampled directly on the ground. The simultaneously unsupervised clusters were also overlaid on the Google Earth high resolution base images to identify the class using image interpretation keys. In addition, 1009 randomly sampled Google Earth points were used for the purpose of accuracy assessment of the GMRCA.

2.3.3. Degree confluence project data

The degree confluence project (http://www.confluence.org) is a voluntary effort of organized sampling of the entire World at every 1-degree latitude and longitude intersection. The confluence points have precise latitude, longitude, and a digital photo. We used DCP data, putting the entire dataset in a geographic information systems (GIS) format to interpret land use at each location based on the digital photo. Initially, we have downloaded over 6000 DCP field-plot data points across the globe. We have each point data with proper LULC based on the detail description provided by the visitor who collected that particular point. Unfortunately every field-plot point data does not have detail description about the factors such as the land

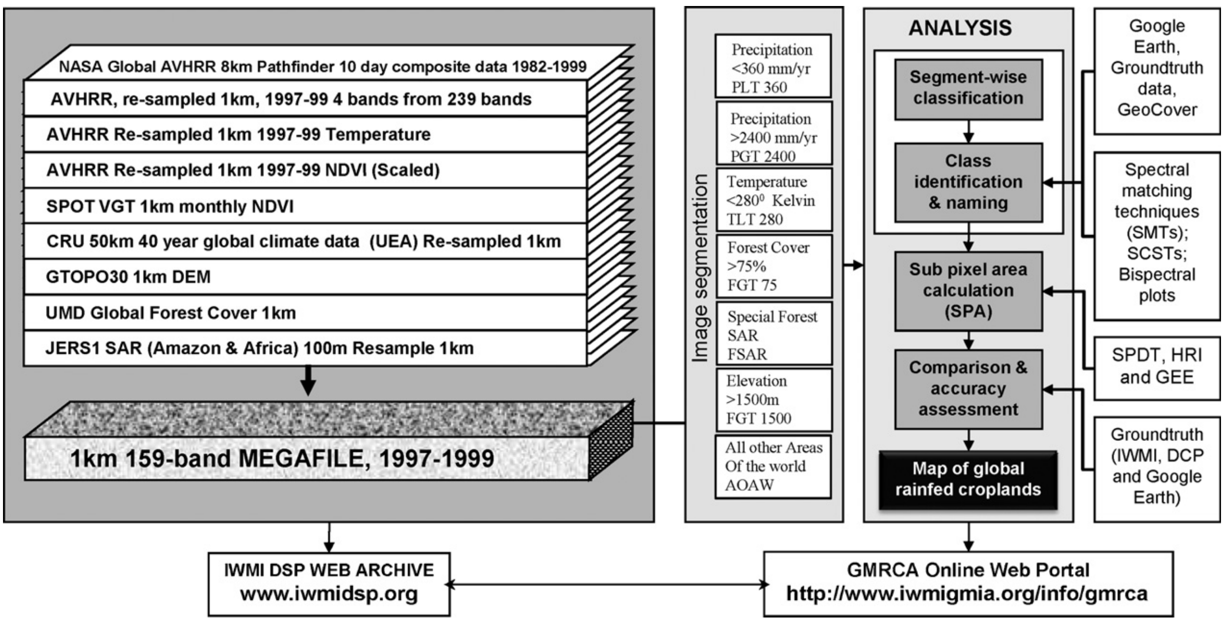

Fig. 1. Distribution of field-plot data points across the World. The field-plot data points were obtained from two sources: (a) field-plot campaigns specific to the project, and (b) degree confluence project (http://www.confluence.org/).

use, agriculture, irrigated, or rainfed. So we have dropped many points whose description is insufficient to label the type of the LULC class. Finally we were left with only 3982 confluence points that had detailed LULC type, precise latitude, longitude, and digital photos.

The above three unique field-plot data (Sections 2.3.1–2.3.3) were pooled together and their spatial distribution shown in Fig. 1. All field-plot data were converted to proprietary geographic information systems formats and were made available publicly through IWMIDSP.

3. Methods

The basic process involves composing mega-file data-cube datasets (Fig. 2), segmenting the world into characteristic regions that were easier to analyze, performing an unsupervised classification on each segment, grouping similar classes through spectral matching techniques (SMTs), setting up a class identification and labeling process (Figs. 3 and 4), resolving the mixed classes (Fig. 5), and calculating the sub-pixel areas (SPAs) (Fig. 6). Class naming is standardized with earlier global land cover classifications (Thenkabail et al., 2008), as far as possible. The specific methods are discussed in the following sections.

3.1. Segmenting the World into characteristic regions

The original 159 band mega-file data-cube was converted into a mega-file of segments, each with its own set of 159 bands (see Fig. 2). In order to create MFDC segments, we will first need to create masks. The seven global masks are:

- Precipitation less than 360 mm per year (PLT360);
- Precipitation greater than 2400 mm per year (PGT2400);
- Temperature less than 280 K per year (TLT280);
- Forest cover greater than 75% canopy cover (FGT75);
- Special forest SAR (FSAR);
- Elevation greater than 1500 m (EGT1500); and
- All other areas of the World (AOAW).

Masks are achieved by taking the secondary datasets such as precipitation, elevation, and temperature and applying simple algorithms in ER-Mapper. For example, in order to create a mask of areas greater than 1500 m elevation, first the elevation data layer is displayed on the screen using ER-Mapper software (or other similar software). This is followed by applying a code in ER-Mapper such as:

If elevation > 1500 then i1 else null

This will retain areas greater than 1500 elevation and makes all other areas null (zero). Thus the areas of the world with 1500 m or higher elevation are available as a mask. This mask (EGT1500) is used to overlay on the MFDC (Section 2.2) and create a new mega-file of only areas of the World greater than 1500 m elevation. The same process is repeated for creating MFDC segments of other segments.

Segment based classification and class identification is very helpful for rapid identification of classes. For example, we can be almost certain that there is little or no agriculture possible in areas with temperature less than 280 K. So when the MFDC of TLT280 is classified into few hundred classes, each of these classes is unlikely to be agriculture and certainly not irrigated. In contrast, the classes with high vegetation amongst the classes generated from the PLT360 are likely to be irrigated. Certainly any agriculture in this area is irrigated. So, identification and labeling of classes becomes simpler by taking a segment based classification and class identification approach.

3.2. Spectral matching techniques to group classes

Class signatures (e.g., Fig. 3b and c) were generated based on classification of various MFDC image segments as a function of temperature, elevation, and precipitation (Fig. 2). Class signatures were based on time-series NDVI derived from AVHRR\VGT. For each segment, 100–250 classes were generated using unsupervised classification algorithms (ISODATA clustering) and when a particular class was mixed, the area of this mixed class was masked and re-classified. For all segments, maximum of 250 classes were attempted. However, for certain segments we got less than 100 classes using ISOCLASS clustering based on how many unique classes a maximum likelihood classified could classify. Classes were considered mixed, when it was not possible to definitively identify these classes after going through class identification and labeling protocols described in Sections 3.2.1–3.2.3. Mixed classes were resolved as described in Section 3.4.

3.3. Class identification and labeling

The class identification and labeling process involved the use of spectral matching techniques (Section 3.3.1), bi-spectral plots

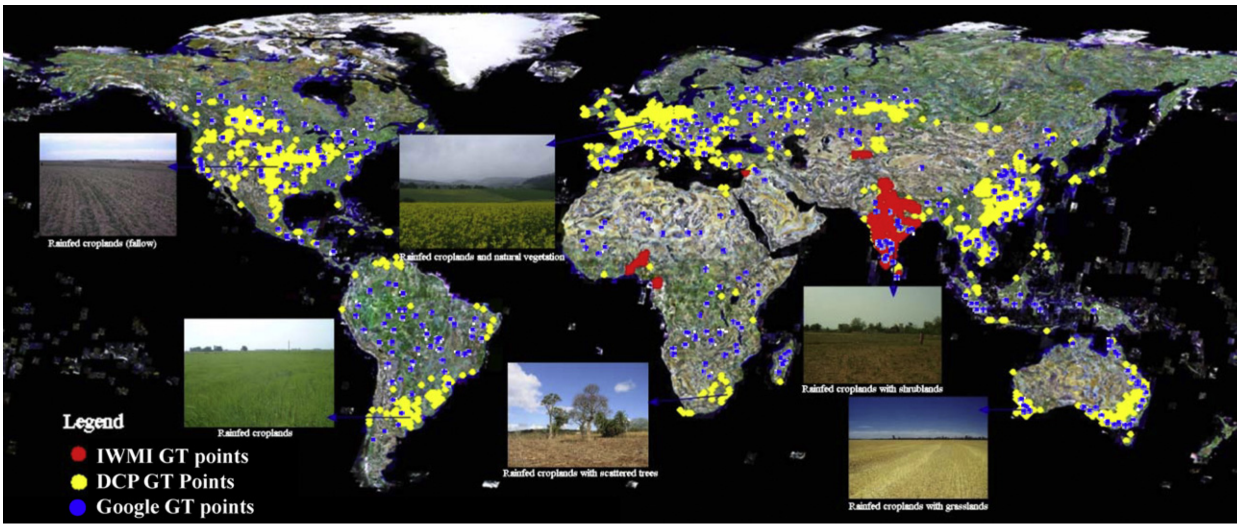

Fig. 2. Flow chart for the global map of rainfed cropland areas (GMRCA).

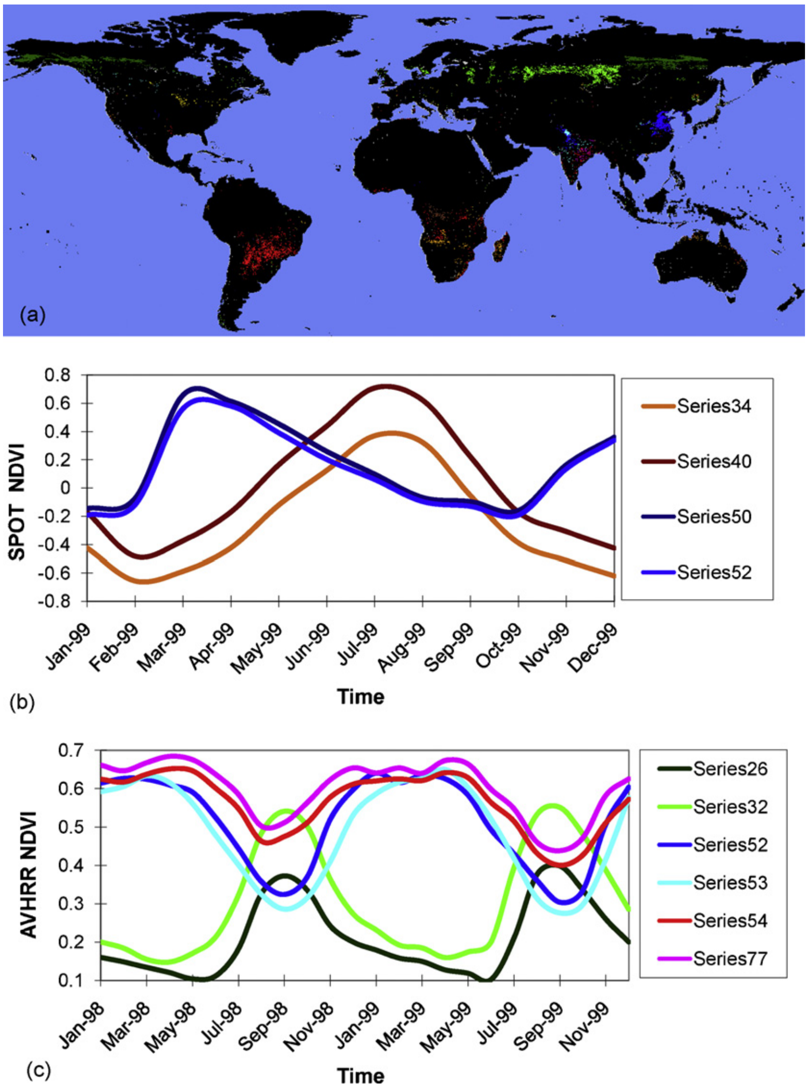

Fig. 3. Class identification and labeling process based on time-series spectra of class. The classes generated (a) by classifying the multiple-sensor mega-file data are identified and labeled based on several approaches described in this paper. One such method is illustrated here where classes are identified and labeled based on time-series characteristics of classes in: (i) SPOT VGT (b) and (ii) AVHRR (c). The classes 34 and 40 and classes 50 and 52 had similar time-series SPOT NDVI with R^2-value >0.95. The classes 50 and 52 match very well in both shape and magnitude. However, class 34 matches class 40 in shape, but not magnitude.

(Section 3.3.2), Google Earth very high resolution imagery (Section 3.3.3), and field-plot data (Sections 2.2 and 2.3). It is possible to determine a class by using any one of these techniques or we may need some or all of them. For example, field-plot data may identify a particular class without any margin for error (e.g., 40 out of 40 points showing a class as a particular type or in the least an overwhelming proportion of points falling into a single class). When there is ambiguity, we may use other methods to provide supporting evidence that the class indeed belongs to a particular type or it is indeed mixed.

The first step in class identification and labeling was done using spectral matching techniques (Homayouni and Roux, 2003; Thenkabail et al., 2007b). The SMTs groups classes with similar spectral characteristics (e.g., Fig. 3b and c). The spectral correlation similarity (SCS) R^2-squared values which identifies and matches classes with similar shape of time-series spectra (e.g., NDVI, surface reflectivity) were used to group classes (e.g., Fig. 3b and c) whose spatial distribution was illustrated in Fig. 3a. For example consider SPOT VGT NDVI values of four classes. The classes 34 and 40 (Fig. 3b) had an SCS R^2-value of >0.95. Similarly classes 50 and 52 were highly correlated with R^2-value of >0.95 (Fig. 3b). This implies that these classes are similar and can be merged. This is especially so for classes 50 and 52 since the NDVI time-series spectra of these classes match both in terms of shape and magnitude. In case of classes 34 and 50, there is a shape match, but not magnitude. This implies, before combining these classes further investigation (Sections 3.3.1–3.3.3) is needed to ensure the classes are of similar characteristics. The quantitative SMTs facilitate identification of a group of similar classes and are a powerful first step in class identification and labeling.

3.3.1. Using ideal (or target) spectral data bank (ISDB)

The ideal or target spectral data bank was created based on field-plot data points of: (a) this project (Sections 2.3, 2.3.1 and 2.3.2), and (b) degree confluence project (Section 2.3.3). The ideal or target spectra were generated by precise knowledge of a class through field-plot and generating the time-series class signature (NDVI or surface reflectivity) using mega-file data-cube. For example, a class such as "rainfed, single crop, season 1" is established based on numerous NDVI spectral signatures of such a class gathered from spatially well distributed points. The class spectra were generated from ISOCLASS unsupervised classification. Spectral correlation similarity R^2-values were used for matching

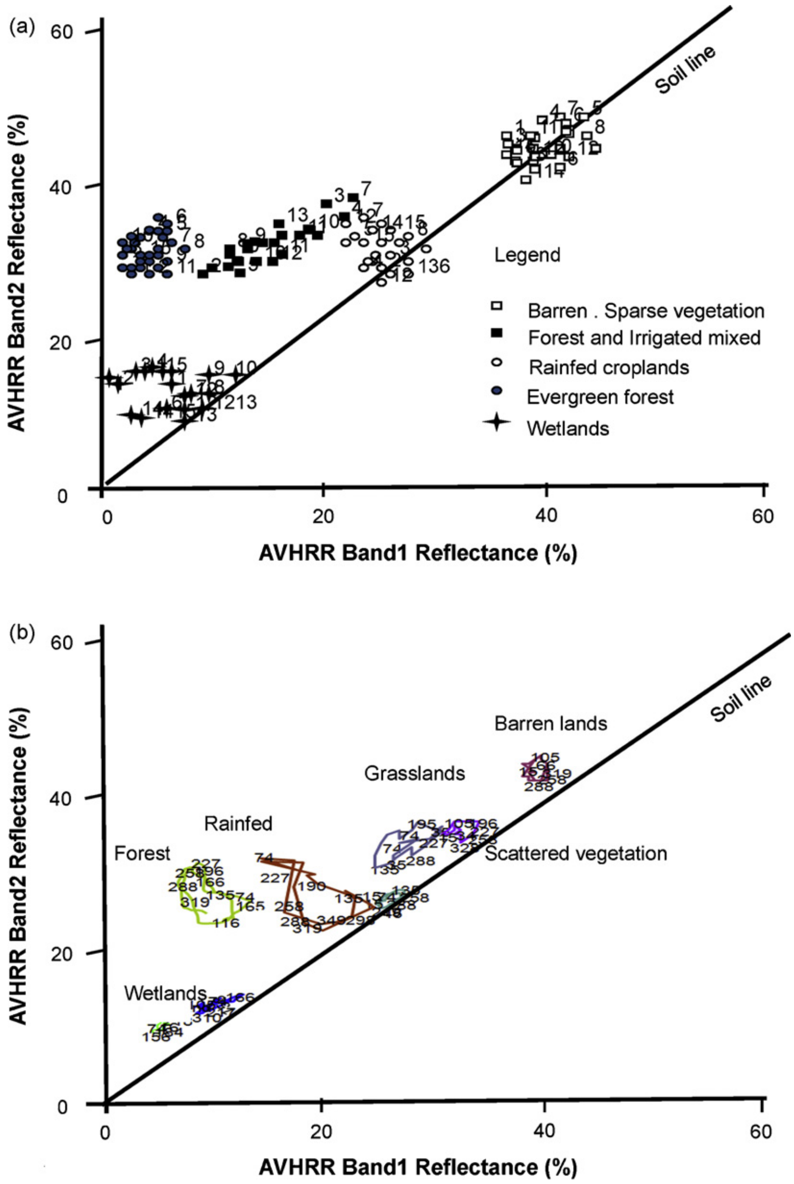

Fig. 4. Class identification and labeling process based on bi-spectral plots and space-time spiral curves. The class spectral characteristics are depicted in 2-dimensional bi-spectral plots (a) and identified and labeled based on combination of their location in spectral space and through field-plot knowledge. The time-series characteristics of the classes are also depicted in 2-d plots in which every class moves through a "territory" in a calendar year and these characteristics are referred to as space-time spiral curves (b).

the class spectra with ideal spectra. The 100s of classes of class spectra were matched with each ideal spectrum to see how many classes of class spectra match with different ideal spectra (e.g., Fig. 3b). Using SCS R^2-values makes this matching an automated process. The SCS R^2-values are shape measure. Typically, when SCS R^2-values between ideal spectra and class spectra was >0.80 then we considered the classes as having close similarity. Once this was the case, the class spectra in consideration were further investigated using Sections 2.3.1–2.3.3 before firmly labeling the class spectra. It is possible to have both shape and magnitude measure by using Spectral Similarity Value (SSV) (Thenkabail et al., 2007b). For a detailed explanation of SMTs, please refer to Thenkabail et al. (2007b).

Theoretically, all classes in class spectra generated from unsupervised classification should have an ideal or target spectra. However, the ISDB is not often as comprehensive to include all classes. And hence only a certain percentage of classes were identified and labeled directly by using the ISDB.

3.3.2. Using bi-spectral plots and space-time spiral curves (ST-SCs)

The 2-dimensional (2-d) bi-spectral plots (e.g., Fig. 4a), and ST-SCs (e.g., Fig. 4b) were useful in class identification process when used in conjunction with field-plot data (Sections 2.2 and 2.3). The ST-SCs (Fig. 4b) depict time-series characteristics such as band reflectivity (Fig. 4a and b) of a class in 2-d feature space (2-d FS). Each class has a territory in which they move around every year. They may have completely distinct territories or may criss-cross each other during certain periods of the year. The advantage of ST-SCs is the time component as we can track class movement in 2-d FS continuously over a season or a year. In contrast the bi-spectral plot is limited to a single date event of class characteristics. Classes such as rainfed and forests have the largest territories in contrast to low and scattered vegetation classes (barren and wetlands) (Fig. 4b). We have this approach to match and group classes that are falling within similar ST-SC plots and have usually characteristic territory that leads to more precise interpretation of the nature of the class (based on sound field knowledge of at least one

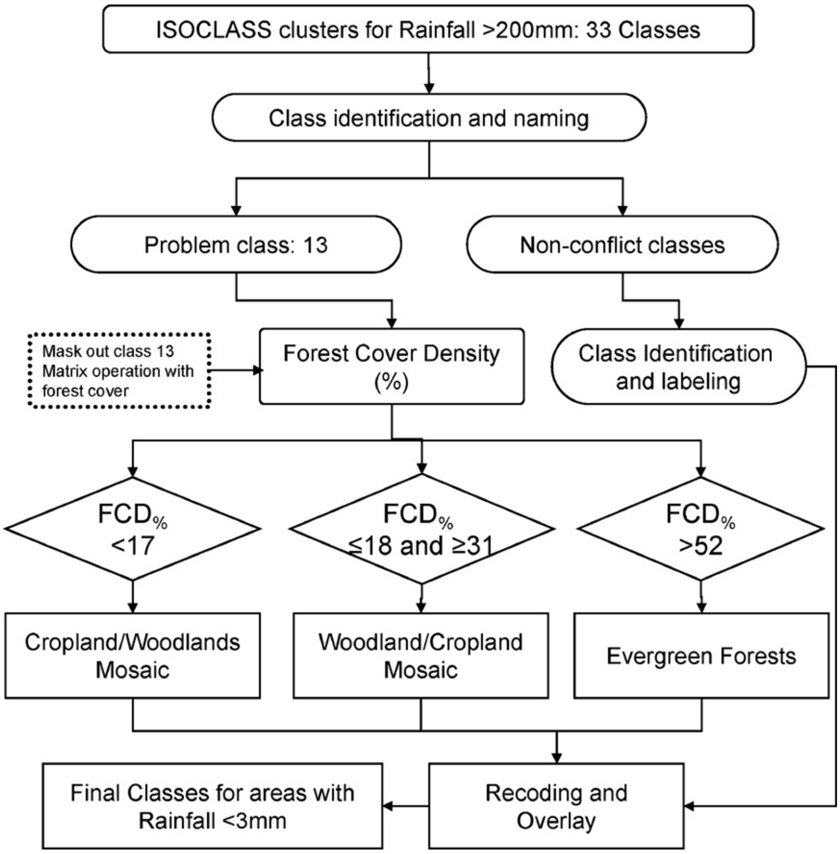

Fig. 5. Resolving the mixed classes. The mixed classes are resolved through decision tree algorithms (illustrated using principal component analysis or PCA in this figure).

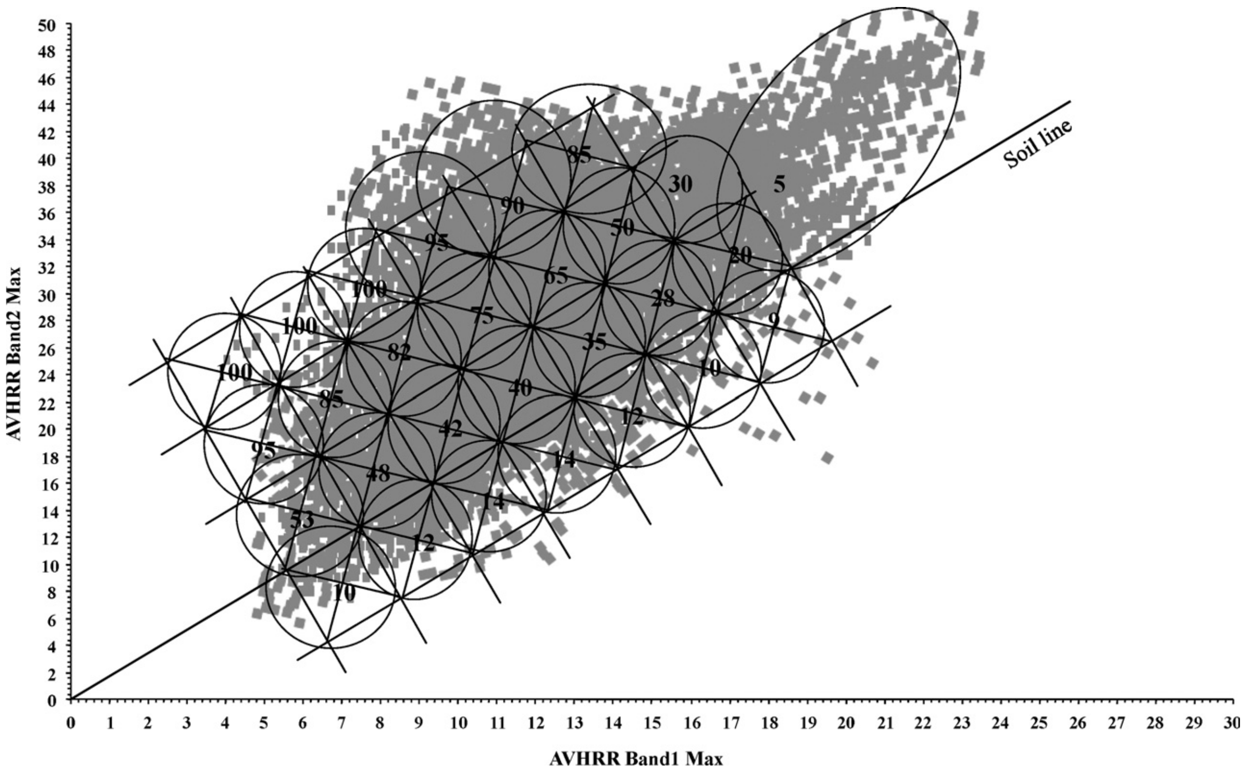

Fig. 6. Sub-pixel area (SPAs) calculations. The rainfed cropland areas were established using SPAs using the three robust methods (Thenkabail et al., 2007b). The sub-pixel decomposition technique (SPDT) is illustrated here for the class1. Every pixel of a rainfed class is depicted in a 2-dimensional red versus near band reflectivity plot (e.g., this figure). Based on where the pixels fall on a 2-d plot, percentages are assigned.

or more classes in a group). In Fig. 4b, rainfed areas have the largest "territory" because it's high variation in vegetation growth from the sowing to peak vegetation/flowering and harvesting. It is important to know the spatial distribution of the class and field-plot knowledge to be definitive of the class name. The ST-SCs provide very good indications of the classes based on where they occur and their "territorial" characteristics (Fig. 4b). The 2-dimensional spectral characteristics of the classes that need to be identified are depicted in the bi-spectral plots (e.g., Fig. 4a) and through space-time spiral curves (Fig. 4b). The specific location of a class in 2-d feature space was indicative of the class type that was further verified using field-plot data reported in Sections 2.2 and 2.3. Also, when classes cluster in specific location of the 2-d FS, all the clustered classes are likely to be similar classes.

3.3.3. Using Google Earth and field-plot data

About 11,000 Google Earth very high resolution imagery zoom-in-views were used in class identification and labeling. In addition, nearly 6000 field-plot points from this project and sourced from degree confluence project were used. The Google Earth field-plot and field-plot data from various sources were used in two ways to identify and label classes as described in Section 3.3.4.

3.3.4. Final labeling of classes

Class labeling is a systematic procedure. First, classes were initially grouped using SMTs and identified using ISDB (Section 3.3.1). Second, initial identification also involves bi-spectral plots and ST-SCs plots (Section 3.3.2). These two steps will lead to preliminary labeling. Third, GE-FP and field-plot data were used for the purposes of further identification and verification. For every class, 30–60 Google Earth very high resolution "zoom-in-view" sample locations were investigated. For each investigated point a class name was given based on image interpretation techniques such as shape, size, texture, location, and proximity to water sources. If an overwhelming majority of the classes were named as a single class (e.g., rainfed), then the class name becomes clear. If there were more than one possible name, then the class was further investigated using field-plot data and resolved. In many ways, Google Earth data is similar to field-plot data and in some cases, even better because it provides spatial view that is not provided by field-plot data. Fourth, field-plots were used either to exclusively identify classes or to provide supportive and definitive evidence of the class labeling during any of the steps one through three. Overall, it is better to integrate these methods to identify and label classes.

3.4. Resolving mixed classes

In spite of rigorous methods of class identification and labeling (Sections 3.3.1–3.3.4), some classes remain unresolved due to presence of more than one class within a class. When a global level classification is performed using ISOCLASS clustering algorithm, we may specify 250 classes (maximum possible using ERDAS Imagine software) for every segment. However, some of these classes actually have several sub-classes within a broad class. For example, we will have irrigated crop mixed with rainfed crop. We can separate this by several ways. First, we can take one of this mixed classes, use it as a mask to further segment a MFDC, re-classify this area, and obtain several classes. When such an approach is used, we may be able to separate originally mixed rainfed class from irrigated class and so on. There are other approached of resolving the mixed classes by employing decision tree algorithms (Defries et al., 1998), and spatial modeling (Thenkabail et al., 2006, 2008).

In mask and re-classification approach, mixed class areas were overlaid on image file and the areas masked out. Such an image area was then re-classified and the process of class identification and labeling (Section 3.3) were repeated. In the second method, decision tree algorithms (e.g., Fig. 5) were used to resolve classes. For example, in Fig. 5, we illustrate a mixed class areas for which a principal component analysis (PCA) image was taken, classified using unsupervised classification, and a decision tree code written to identify and label classes. In the third method, we take the mixed classes and perform GIS spatial analysis to resolve the classes. We have used secondary datasets such as elevation, aspect, slope, evapotranspiration to GIS modeling to separate mixed pixels of two or more classes. For example, a mixed class having pixel of forest and croplands, we used slope as a criteria and assumed that cropland are usually not at slope more than 20% and forest can occur even more than 20% slope. The mixed class (forest and cropland) is multiplied with slope map to segregate the mixed pixels into forests and croplands.

3.5. Sub-pixel area calculations

It is now well known that accurate estimates of areas from coarse resolution imagery can only be achieved based on sub-pixel areas. The two established SPA calculation techniques and methods are described in Thenkabail et al. (2007a) and Biggs et al. (2006). We adopted these methods to calculate precise rainfed areas. The sub-pixel rainfed cropland areas were calculated by multiplying full pixel areas (FPAs) of that pixel with rainfed area fractions (RAFs). The RAFs were determined by using three methods (Thenkabail et al., 2007b): (a) Google Earth Estimates (GEE), (b) high resolution imagery (HRI), and (c) sub-pixel decomposition techniques (SPDT). Of these three methods, SPDT is automated and relatively fast. The SPDT involves plotting the reflectivity of red versus near-infrared (Kauth and Thomas, 1976) for every pixel in a class in a feature space. Depending upon the pixel location in the feature space plot, the percent area cultivated was determined, providing us with RAFs. A detailed explanation of deriving sub-pixel area fractions is provided in Thenkabail et al. (2007b). So we refer the reader to this paper.

In this study, we used the RAFs derived from the three methods and used an average of the three methods to come to a final RAFs (Table 2). When RAFs of two methods for a class were significantly different ($\pm$0.05) then we re-investigated the class for RAF to ensure that the two methods had significantly similar RAFs. This we had to do for three of the nine classes.

4. Results and discussions

The final outcome is an aggregated 9-class global map of rainfed cropland areas (Fig. 7). The class names indicate (Table 2 and Fig. 7): (a) rainfed classes with little or no other classes mixing with them (classes 1 and 2), (b) significant rainfed classes with mix of grasslands, shrublands, or woodlands (classes 3–5), (c) dominant grasslands, shrublands, and woodlands, with moderate or low levels of rainfed croplands (classes 6–8), and (d) dominant forest lands with significant fragments of rainfed croplands (class 9). The non-rainfed classes were not mapped and were shown in light gray. All classes have mixed crops, at 1–10 km resolution this is unavoidable. Crop dominance for the first two classes was determined based on field-plot data (Table 2). The total rainfed cropland area from all nine classes was 1.13 Bha; of this the first two classes have 36.5%. These two classes were predominantly rainfed croplands with very little other land use. The rainfed area fractions were little over 50% for classes 1 and 2, between 34–40% for classes 3–5, and between 12–25% for classes 6–9 (Table 2). Every rainfed cropland class (or every pixel within a class) has its own characteristics in terms of its vegetation dynamics, seasonality, topographic location, and biophysical properties. The

Table 2
Areas of global map of rainfed cropland areas (GMRCA) classes. The areas are computed by taking the full pixel area (FPAs) and multiplying the same with the rainfed area fraction (RAF). The SPAs provide the actual areas.

Class number	Class name	Full pixel area (ha)	RAF* (ha)	SPA# (ha)	Percent of total area	AVHRR NDVI
1	Rainfed croplands (corn, soybeans, and wheat dominant)	423,204,269	0.55	232,762,348	20.57	0.39
2	Rainfed croplands (wheat, cotton, and barley dominant)	348,389,483	0.52	181,162,531	16.01	0.43
3	Rainfed croplands and grasslands	569,862,800	0.37	210,849,236	18.63	0.43
4	Rainfed croplands and shrublands	69,362,335	0.34	23,583,194	2.08	0.43
5	Rainfed croplands and woodlands	150,842,832	0.40	60,337,133	5.33	0.27
6	Grassland dominant with rainfed croplands	900,008,806	0.25	225,002,201	19.88	0.32
7	Shrublands dominant with rainfed croplands	416,508,118	0.13	54,146,055	4.79	0.32
8	Woodland dominant with rainfed croplands	359,324,051	0.17	61,085,089	5.40	0.58
9	Forest dominant with rainfed croplands	671,021,180	0.12	82,624,536	7.30	0.26

Note: * = RAF: rainfed area fraction; # = SPA: sub-pixel area.

dynamic properties of an individual class allows one to study variables such as cropping calendars, crop growth stages, biomass levels, and rainfed fractions.

There was also a disaggregated GMRCA map with 66 classes, not presented in this paper, which was made available for download from the web portal (http://www.iwmigiam.org/). This map will be specifically useful for those interested in creating more refined class maps for their areas of interest.

4.1. Global rainfed and total cropland area

The total global rainfed cropland area was determined as 1.13 Bha (Table 2 and Fig. 7). The total cropland areas were estimated at 1.53 Mha (Table 3) by adding rainfed cropland areas of this study (Table 3 and Fig. 7) and the irrigated cropland study of Thenkabail et al. (2006, 2008) for the year 1999 (Fig. 8). These results compare very well with the cropland areas estimated in the FAOSTAT (2000) which was based on country statistics (Table 5 and Fig. 9a and b). Literature shows that the World's croplands (rainfed plus irrigated) around the end of the last millennium was anywhere between 1.11 and 3.62 Bha as reported in various studies (Table 4). Most global digital maps (e.g., Loveland et al., 1999; Olson and Watts, 1982; Matthews, 1983) over estimate agricultural areas as a result of the full pixel based area calculations (Xiao et al., 1997; Cramer and Soloman, 1993). A pixel when classified as agriculture is automatically taken to have 100% croplands in digital global maps. In reality only a certain percentage of a pixel is in cropland and that percentage can vary substantially. This is specially so in most developing countries where cropland areas are highly fragmented and mixed with other land use/land cover. As a result, the total agricultural lands estimated in various digital maps were 2.7 Bha by Olson and Watts (1982) using a 50-km grid, 3.2 Bha by Matthews (1983) using 100-km grid, and 2.8 Bha by IGBP and USGS using 1-km grid (see Loveland et al., 1999). The FAOSTAT (2000) estimates at 1.51 Bha for year 1998 and Tilman et al. (2001) estimated 1.54 Bha for the nominal year 2000. Our estimate for the year 1999 (1.53 Bha) falls between the immediate above two estimates. A country-by-country comparison between total cropland area estimated by this study with agricultural census dataset from the FAOSTAT shows the linear relationship (R^2 = 0.94; n = 182; Fig. 9). The root mean squared error between these two datasets at the national level is ~6 Mha. There was some degree of similarity in spatial distribution of cropland areas. The FAO statistics show cultivated areas at about 1.51 Bha (FAO, 2002; Table 4). Grubler (1994) estimated that an increase of 1 billion arable lands would

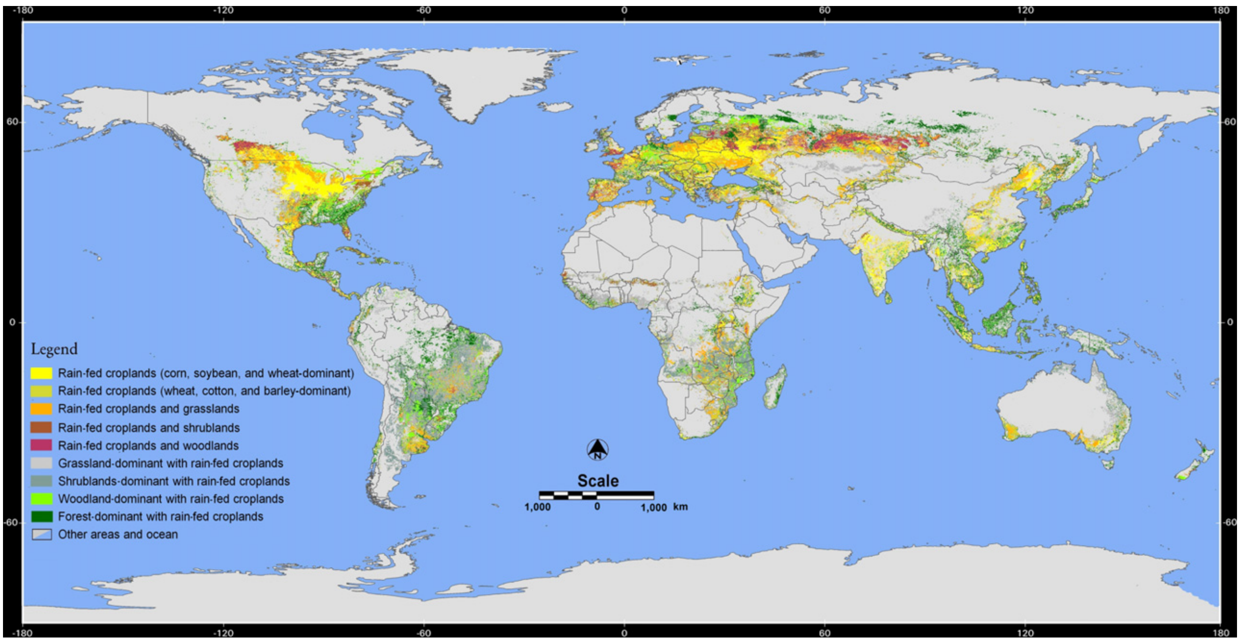

Fig. 7. Global map of rainfed cropland areas (GMRCA). This is a 9-class GMRCA map at nominal 1-km resolution produced using a fusion of 1-km SPOT VGT, 10-km NOAA AVHRR, and numerous secondary data. The first five classes are dominated by rainfed classes, the next three are dominated by savannas with significant rainfed croplands, and the class 9 is dominated by forests with significant rainfed cropland fragments.

Table 3
Cropland areas of the continents and the World. The rainfed, irrigated, and the total cropland areas for the continents and the World.

Sl. no.	Continents (name)	Irrigated area (Million ha)	Rainfed area (Million ha)	Total cropland area (Million ha)
1	Africa	8.69	189.05	197.74
2	Asia	290.64	327.29	617.93
3	Australia	11.87	36.76	48.63
4	Europe	33.94	227.89	261.83
5	North America	35.43	190.67	226.10
6	Oceania	17.84	1.46	19.30
7	South America	0.13	158.44	158.57
	Total	398.53	1131.56	1530.09

be needed for additional 5 billion world population in the 21st century.

The geographical distribution of the total rainfed cropland area estimated in this study was closely correlated with the geographical distribution of human population. The high percent of total rainfed croplands occur mostly in countries with high population. The United States, Russia, China, Brazil and India, account for the highest rainfed cropland areas in the world. However, per capita rainfed areas in Indian and China were quite low as compared to rest of the top five rainfed nations. Rainfed croplands were often inferred and are not reported directly. For example, the FAOSTAT (2000) reports total croplands as 1.51 Bha without any indication of the break-up between rainfed and irrigated areas. The FAO and the University of Frankfurt study (Siebert et al., 2006) reported global irrigated areas as 278.4 Mha. In an earlier study, Thenkabail et al. (2008) reported the total global net irrigated area was 399 Mha (Table 2). The FAOSTAT (2000) estimates at 1.51 Bha for year 1998 and Tilman et al. (2001) estimated 1.54 Bha for the nominal year 2000. Our estimate for the year 1999 (1.53 Bha) falls between the above two estimates. The causes of these differences were due to: (a) methods and approaches employed, (b) definition of irrigated and rainfed areas (e.g., supplemental areas are at times mapped as irrigated and at other times mapped as rainfed), (c) accounting or non-accounting for informal irrigation (e.g., ground water, small reservoirs, and tanks as irrigated), (d) uncertainties in rainfed area fractions, and (e) resolution (or scale) of the imagery used.

4.2. Continental rainfed cropland area statistics

Of the 1.13 Bha (Table 3) of rainfed croplands in the World, Asia dominates with 29%, followed by Europe (20%), North America (17%), Africa (17%), South America (14%), and Australia (3%) (Table 5).

The total cropland area of the world has not changed significantly compared to population growth. Compared to the early 1960s and the late 1990s, the world cropland grew by only 11%, while world population almost doubled. As a result, cropland per person fell by 40%, from 0.43 ha to only 0.26 ha and reduced from 0.23 to 0.11 ha (FAO, 2002). Much of the increased food production has come from the green revolution involving higher yielding grain varieties, and rapid expansion of irrigated areas. The increased population and little or no scope for further expansion of the cropland areas without significant environmental damage requires us to think anew on strategies for higher food production in from the available agricultural lands and available water. In the future, approximately 80% of increased crop production in developing countries will have to come from intensification: higher yields, increased multiple cropping, and shorter fallow periods.

4.3. Country rainfed cropland areas and a summary of rainfed, irrigated, and total cropland areas

The cropland area statistics are provided for the 182 countries (Table 6) and total cropland area compared with FAO statistics (FAOSTAT, 2000). Table 6 is arranged based on the ranking of the global cropland areas (rainfed plus irrigated). It is obvious that some of the countries like India and China have overwhelming dominance of irrigated areas (Table 6), but have relatively low rainfed areas (Table 6). The rainfed croplands (Fig. 8) are dominant in the United States (11.8% of 1.13 Bha), followed by Russia (10.1%), China (8.1%) Brazil (7.72%), India (4.31%), Australia (3.25%), Canada (3.09%), and Argentina (3.03%). These eight countries have 51.4% of all global rainfed croplands. There are 12 countries between 1.1 and 2.8%. The rest of the countries have less than 1% of the total

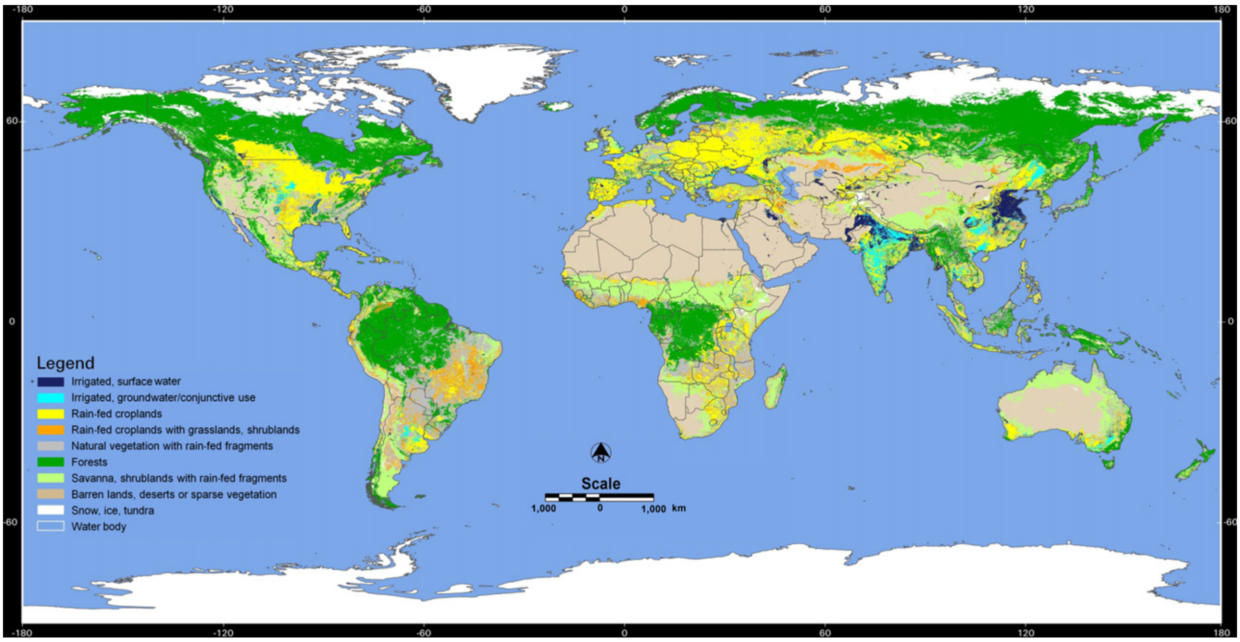

Fig. 8. Global rainfed croplands along with irrigated crops and other land use/land cover. The classes 1 and 2 are irrigated croplands, classes 3 and 4 are rainfed croplands, class 5 is natural vegetation with significant rainfed fragments, and the rest of the classes are non-croplands (http://www.iwmigiam.org).

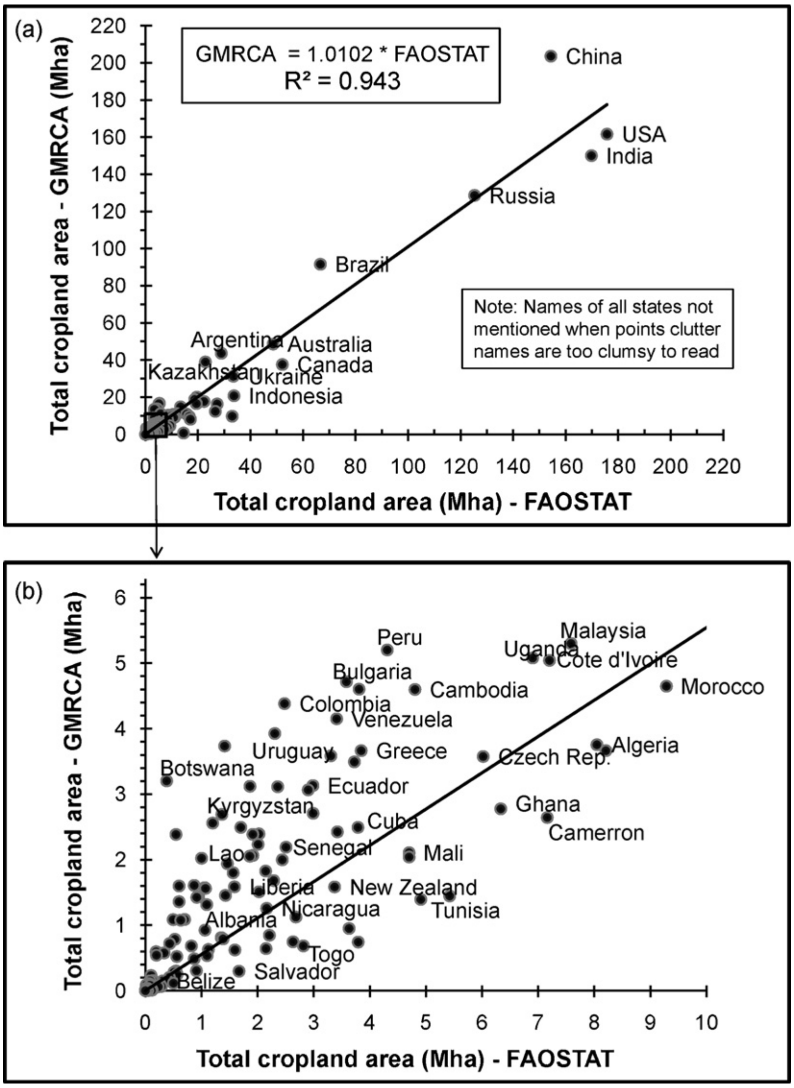

Fig. 9. Global total cropland area estimated from this study is compared with FAOSTAT data compiled from national agricultural census data.

global rainfed cropland areas. The first 20 countries account for 70% of all rainfed croplands and first 40 countries account for 84.2% of all rainfed croplands (Table 6). Roughly one third of the World's population lives in two countries. China and India are the most populous countries in the world with only 23% of the total cropland area. The geographical distribution of the total rainfed cropland area estimated in this study is closely correlated with the geographical distribution of human population. The high percent of total rainfed croplands occur mostly in countries with high population. The United States, Russia, China, Brazil and India, account for the highest rainfed cropland area in the world. However, per capita rainfed area in Indian and China is quite low as compared to rest of the top five rainfed nations.

Table 4
Cropland areas of the World estimated from various sources. The cropland areas (rainfed + irrigated) of the World estimated from different sources for the end of the last millennium shows huge differences from one source to another.

Total cropland area (Bha)	Year	Source
1.11	2000	Hansen et al. (2000)
1.34	1994	Warnant et al. (1994)
1.36	1999	Houghton (1999)
1.39	1999	Loveland et al. (2000)
1.40	1991	FAO (1990, 1991)
1.48	2001	Goldewijk (2001)
1.48	1998	Amthor et al. (1998)
1.50	1991	Lal and Pierce (1991)
1.50	2003	WRI (2003)
1.51	1998	FAOSTAT (2000)
1.53	1999	Our estimation (see Table 3)
1.54	2000	Tilman et al. (2001)
1.60	1998	WBGU (1998)
1.79	1998	Ramankutty and Foley (1998)
2.79	2000	WRI (2000)
3.62	2000	Wood et al. (2000) and WRI (2000)

4.4. Spatial distribution of rainfed cropland areas

The cropland distribution estimate based on this research indicates that 1.5 Bha of the earth's land surface has been put under agricultural crop production (irrigated and rainfed area). This indicates that roughly one third of the total potential area available for crop production is being utilized. There is still a large surface area available for further expansion of agricultural croplands especially in Latin America and Africa. However, expansion of croplands in these regions depends on crop management practices, where soil degradation will determine the success of crop production. Highly populated nations such as China and India have little scope for further expansion or intensification of cropland areas.

Table 5
Country level statistics for annualized irrigated area, rainfed cropland area and total cropland areas. The ranking of the countries based on total cropland areas.

Rank	Countries	Annualized irrigated area[a] (ha)	Rainfed cropland area (ha)	Total cropland area (ha) by GMRCA
1	China	151,802,086	91,635,702	203,624,473
2	United States	24,309,188	133,571,602	161,617,081
3	India	132,253,854	48,824,269	150,059,162
4	Russia	11,203,530	114,788,560	128,675,415
5	Brazil	4,085,844	87,408,556	91,603,674
6	Australia	5,373,409	36,758,302	48,623,546
7	Argentina	8,766,412	34,318,900	43,623,158
8	Kazakhstan	6,469,685	31,722,986	38,950,704
9	Canada	2,874,252	34,944,402	37,602,699
10	Ukraine	2,381,799	28,290,153	31,285,731
11	Indonesia	3,322,443	17,573,608	20,746,487
12	France	2,687,153	17,648,821	20,048,339
13	Spain	3,025,823	15,392,046	18,813,770
14	Pakistan	15,959,342	3,642,557	17,678,708
15	Zambia	536	16,677,106	16,677,885
16	Thailand	7,397,368	9,931,747	16,542,332
17	Tanzania	46,998	16,410,652	16,457,674
18	Mexico	3,608,730	12,497,923	16,352,595
19	Congo, DPR	20,375	15,815,336	15,837,169
20	Poland	454,111	14,424,037	14,775,550
21	Mozambique	60,742	13,726,544	13,782,960
22	Angola	34,158	13,454,118	13,477,434
23	Turkey	1,577,313	10,603,366	12,356,748
24	Germany	3,001,674	8,998,878	11,196,575
25	Belarus	60,926	10,968,114	11,052,202
26	South Africa	828,491	10,097,803	10,918,843
27	Ethiopia	162,808	10,564,343	10,748,582
28	Myanmar	6,306,671	6,257,996	10,710,993
29	Vietnam	4,949,533	5,967,528	10,351,550
30	Romania	2,049,888	7,563,254	9,938,493
31	Nigeria	216,154	9,572,789	9,770,698
32	Sudan	1,930,592	7,816,063	9,553,181
33	Italy	2,644,140	6,436,452	9,265,975
34	Philippines	1,789,108	7,479,645	9,022,274
35	Bolivia	163,036	8,803,829	9,017,920
36	Zimbabwe	3,533	8,781,932	8,786,677
37	Iran	2,488,558	5,509,694	8,133,031
38	Bangladesh	7,166,028	2,536,292	7,771,342
39	Uzbekistan	5,295,515	2,821,987	6,423,474
40	Kenya	104,527	5,944,333	6,029,734
41	United Kingdom	1,060,204	5,014,629	5,985,362
42	Japan	2,468,596	3,428,667	5,953,762
43	Colombia	592,495	5,359,287	5,905,473
44	Paraguay	25,029	5,538,996	5,567,578
45	Madagascar	75,156	5,345,476	5,417,835
46	Malaysia	274,565	5,042,468	5,301,234
47	Peru	374,954	4,846,774	5,202,729
48	Cote d'Ivoire	101,890	4,986,024	5,081,162
49	Uganda	30,586	5,012,869	5,042,886
50	Bulgaria	1,012,064	3,416,518	4,718,322
51	Morocco	1,153,817	3,603,724	4,648,843
52	Cambodia	938,441	3,868,166	4,604,483
53	Hungary	186,221	4,358,475	4,600,188
54	Nepal	1,477,303	3,131,060	4,383,047
55	Venezuela	807,078	3,256,971	4,151,851
56	Chile	1,445,230	2,412,213	3,927,135
57	Afghanistan	923,490	2,748,082	3,756,220
58	Uruguay	360,055	3,354,348	3,735,751
59	Greece	766,678	2,757,498	3,665,237
60	Algeria	136,946	3,520,819	3,665,169
61	Czech Republic	701,727	3,068,209	3,586,245
62	Iraq	2,626,564	1,356,711	3,576,735
63	Botswana	4,278	3,198,620	3,204,037
64	Ecuador	281,166	2,844,430	3,133,011
65	Korea, Rep.	1,313,755	1,928,760	3,121,229
66	Serbia	234,348	2,947,604	3,119,543
67	Portugal	313,908	2,756,177	3,115,042
68	Korea, DPR.	2,053,625	1,598,207	3,065,469
69	Ghana	71,764	2,716,307	2,776,954
70	Lithuania	41,591	2,651,512	2,708,784
71	Kyrgyzstan	770,274	1,990,967	2,691,843
72	Cameroon	52,128	2,591,767	2,644,461
73	Mongolia	376,378	2,136,984	2,559,316
74	Cuba	637,159	2,007,424	2,494,322
75	Guinea	320,350	2,190,800	2,493,433
76	Egypt	3,292,726	281,590	2,425,690

Table 5 (*Continued*)

Rank	Countries	Annualized irrigated area[a] (ha)	Rainfed cropland area (ha)	Total cropland area (ha) by GMRCA
77	Central African Republic	1,086	2,393,214	2,394,369
78	Sri Lanka	809,579	1,439,246	2,387,275
79	Congo	0	2,386,480	2,386,480
80	Azerbaijan	821,980	1,398,784	2,234,411
81	Senegal	290,572	1,980,242	2,191,659
82	Mali	65,879	2,051,073	2,107,428
83	Turkmenistan	1,999,984	542,979	2,065,350
84	Latvia	7,325	2,040,565	2,053,248
85	Burkina faso	14,660	2,025,961	2,041,623
86	Laos	107,734	1,917,269	2,022,854
87	Malawi	2,794	1,996,142	1,999,435
88	Austria	98,551	1,822,194	1,938,650
89	Moldova	229,433	1,533,012	1,827,082
90	Slovakia	75,488	1,690,815	1,800,719
91	Denmark	979,539	517,119	1,681,824
92	Taiwan, Province of China	677,877	1,111,947	1,610,990
93	Papua New Guinea	0	1,607,752	1,607,752
94	Liberia	300	1,598,806	1,599,043
95	Croatia	44,630	1,551,680	1,586,883
96	New Zealand	141,686	1,459,699	1,585,089
97	Tajikistan	449,153	1,190,392	1,573,635
98	Somalia	403,574	1,189,487	1,561,962
99	Guatemala	91,313	1,440,867	1,510,240
100	Honduras	77,729	1,384,346	1,454,930
101	Syria	596,263	879,249	1,446,239
102	Netherlands	1,011,340	564,102	1,434,345
103	Belgium	507,430	1,101,425	1,426,221
104	Tunisia	100,647	1,284,882	1,394,025
105	Sierra Leone	29,037	1,336,205	1,358,012
106	Bosnia and Herzegovina	14,203	1,303,620	1,314,387
107	Nicaragua	22,720	1,241,957	1,258,396
108	Sweden	71,108	1,040,821	1,124,739
109	Albania	225,864	864,549	1,088,326
110	Panama	45,048	1,037,572	1,086,641
111	Gabon	0	1,084,861	1,084,861
112	Estonia	14,476	1,052,562	1,077,199
113	Chad	27,698	925,287	950,520
114	Georgia	146,141	796,878	925,416
115	Macedonia	131,620	695,920	865,762
116	Finland	71,961	721,148	846,455
117	Burundi	8,490	798,743	810,536
118	Rwanda	64,806	710,557	790,624
119	Costa rica	15,791	772,096	784,724
120	Togo	23,843	725,130	746,856
121	Saudi Arabia	551,066	63,518	742,196
122	Switzerland	36,976	690,849	720,372
123	Niger	4,317	703,697	707,826
124	Benin	15,415	668,742	683,915
125	Namibia	9,303	672,697	683,224
126	Libya	210,022	412,158	642,814
127	Ireland	0	630,766	630,766
128	Dominican Republic	79,648	550,415	621,291
129	Swaziland	97,004	446,942	596,216
130	Lesotho	3,681	571,627	577,303
131	Slovenia	510	542,220	542,659
132	Haiti	53,903	486,161	537,009
133	Armenia	118,324	415,591	522,285
134	Norway	1,453	485,336	487,408
135	Montenegro	13,908	364,360	374,691
136	El Salvador	10,401	294,667	306,258
137	Guinea-Bissau	155,389	191,959	300,001
138	Yemen	79,188	206,310	297,998
139	Guyana	102,930	184,027	280,303
140	Eritrea	13,776	232,850	249,868
141	Thegambia	63,415	197,119	236,991
142	Belize	3,510	228,077	231,964
143	East Timor	4,061	222,063	225,863
144	Israel	104,542	101,665	201,470
145	Cyprus	4,863	148,942	156,041
146	Bhutan	1,396	154,068	155,065
147	Lebanon	25,268	126,708	151,455
148	Puerto Rico	11,253	138,701	150,664
149	Jordan	52,541	75,548	148,266
150	Mauritania	20,036	100,469	115,592
151	Luxembourg	0	111,041	111,041
152	Suriname	20,774	88,593	108,439
153	United Arab Emirates	70,603	0	93,810

Table 5 (*Continued*)

Rank	Countries	Annualized irrigated area[a] (ha)	Rainfed cropland area (ha)	Total cropland area (ha) by GMRCA
154	Brunei	1,002	86,509	87,308
155	Oman	30,145	66,449	84,302
156	Jamaica	4,556	61,139	66,020
157	West Bank	1,542	64,136	65,748
158	Equatorial guinea	2,644	57,260	60,072
159	Qatar	27,596	0	38,509
160	Kuwait	26,753	0	37,333
161	French Guyana	2,822	18,869	21,729
162	Trinidad and Tobago	1,720	8,590	10,449
163	Singapore	0	8,941	8,941
164	Gaza Strip	6,790	693	6,601
165	Andorra	0	5,776	5,776
166	Mauritius	3,910	0	5,312
167	Liechtenstein	0	4,839	4,839
168	San Marino	797	2,060	3,162
169	Antigua and Barbuda	2,468	0	2,270
170	Guadeloupe	2,022	0	1,894
171	St. Kitts and Nevis	1,445	0	1,650
172	Djibouti	587	0	905
173	Virgin Islands	1,015	0	827
174	Reunion	846	0	651
175	Anguilla	404	0	489
176	Comoros	417	0	241
177	Turks and Caicos Islands	170	0	214
178	Monaco	53	132	206
179	St. Pierre and Miquelon	59	0	70
180	Montserrat	115	0	69
181	Seychells	44	0	66
182	Cayman Islands	55	0	66
		466,757,680	1,131,552,270	1,530,079,274

[a] For irrigated area estimations, refer to Thenkabail et al. (2008).

The spatial distribution of global rainfed croplands relative to global irrigated croplands and other global LULC classes (http://www.iwmigiam.org) are shown in Fig. 8. China and India with about 2.6 billion people mostly depend on irrigation, often double cropping, to feed their populations (Thenkabail et al., 2008). In contrast, North America and Europe, with a combined population of about 1.3 billion depend on rainfed agriculture with only one crop per year. They also export large quantities of their food grains to other continents (Thenkabail et al., 2008). Globally, on an average only 0.26 ha per capita of cropland (including irrigated and rainfed) is available for the food production. The per capita availability of world total cropland area has decreased due to population growth, soil degradation, and salinisation (Thomas and Middleton, 1993; Worldwatch Institute, 2001; Preiser, 2005). In contrast, North America and Europe accounts 0.55 ha per capita cropland area to support the diverse food system. Over 60% of the world population lives in Asia with support of the 40% of the total cropland area. In others words, Europe and North America accounts 16% of the global croplands areas with only 9% of the total population of the world. Asia accounts only 0.17 ha of total croplands area available per capita which is lowest against 0.26 of the global average. North America has the highest per capita cropland area of 0.74 ha followed by Europe (0.36), South America (0.31), and Africa (0.26).

4.5. Accuracy assessments

The accuracies and errors were assessed based on pooling two unique and independent datasets that were not used during the class identification and labeling process. A total of 1924 field-plot data points were used in class accuracy assessment. First, the 915 field-plot data points reserved for accuracy assessment from GMRCA field campaigns were pooled and the accuracy was assessed. Second, the 1009 randomly generated field-plot data points were also used separately. Finally, all the points from field-plot and Google Earth were pooled and an accuracy assessment was conducted using 1924 points. Table 6 shows accuracy of the rainfed croplands with errors of omission and commission. Accuracy of the rainfed croplands found varied between 92 and 98%. However, the errors of omissions were 2–8% and errors of

Table 6
Accuracy of the rainfed cropland areas of the World. The rainfed classes were assessed for accuracies using data from two sources: (a) IWMI groundtruth (IWMI-GT) data, (b) Google Earth groundtruth (GE-GT) data and (c) combined IWMI and GE-GT data.

Level of accuracy assessment	Total groundtruth sample size of rainfed and non-cultivated areas (#)	Total groundtruth sample size of rainfed areas (#)	Accuracy of rainfed area classes (rainfed GT points falling on rainfed areas) (%)	K_{hat} Coefficient (%)	Errors of omission (rainfed GT points falling on non-rainfed) (%)	Errors of commission (non-rainfed GT points falling on rainfed) (%)
(a) IWMI-GT Data	915[a]	549	92	75.5	8	36
(b) GE-GT Data	1009[b]	647	98	76.0	2	19
(c) IWMI-GT + GE-GT	1924[c]	1196	95	75.6	5	27

[a] Groundtruth (GT) data points of the World for rainfed and non-rainfed areas collected by IWMI. The same data is also used for identification of the disaggregated classes. These are non-independent data sets.
[b] Google Earth groundtruth (GE-GT) data points of the world for rainfed and non-cultivated areas collected by IWMI. The GE-GT points were randomly generated and are completely independent. These 1009 points were not used in class identification and labeling process.
[c] The combined IWMI-GT Data and GE-GT Data. Of the 1924 points, 47.5% of points are also used for class identification process as mentioned in the point a.

commissions were 19–36%. The pooled data from the two sources provided the rainfed cropland accuracy of 94% with errors of omission of 5% and errors of commission of 27% (Table 6). The large error of commission indicates certain fragmented proportion of the other land use/land cover areas were also mapped as rainfed croplands. However, there was a number of fundamental issues related to accuracy assessments at such large scales as 1-km or 10-km resolution pixel size as explained in Thenkabail et al. (2006). First, lack of a complete field-plot data base at the global scale where there are considerable difficulties in field-plotting and establishing the exact percent of rainfed fraction at the pixel size of ~10,000 ha (AVHRR at ~10 km × 10 km). This, typically, lead to the pixel being labeled as rainfed in field-plot data in one corner of the ~10,000 ha pixel, whereas in reality it has some percent of other LULC fragments. Second, satellite sensors capture the average reflectivity from the pixel and hence were influenced by both the rainfed as well as non-rainfed crops within the pixel leading to average spectra for the pixel. This can lead to somewhat higher omission and commission errors. The phenomenon is acute when dealing with pixels of other LULC area (e.g., grasslands, shrublands, etc.) with fragmented rainfed croplands which leads to higher errors of the commission.

5. Conclusions

A global map of rainfed cropland areas was produced and the area statistics determined for the 182 countries for the end of the last millennium using multiple resolution, multiple platform remote sensing at nominal resolution of 10-km.

The study estimated the global rainfed cropland areas as 1.13 billion ha (Bha) at the end of the last millennium. This was 3 times the net global irrigated area which was estimated at 399 Mha by Thenkabail et al. (2008). The total cropland area of 1.53 Bha nearly agrees with the total cropland area reported by FAO (FAOSTAT, 2000) which was compiled from national statistics. A country-by-country 1:1 comparison between the two studies showed an R^2-value of 0.94. Since the FAO (Siebert et al., 2006) study also determines the irrigated areas as 278.4 Mha, their rainfed cropland areas was about 1.26 billion ha which was about 11.7% (130 million ha) higher than the figures reported in this study. The total cropland estimates from various studies found in literature varied from 1.11 to 3.62 Bha compared to 1.53 Bha determined in this study. The differences were as a result of issues such as: (a) methods and approaches, (b) definitions, (c) uncertainties in rainfed area fractions, and (d) resolutions or scale.

Acknowledgements

This study was supported by the International Water management Institute's (IWMI) core funding. We want to acknowledge the vision and support shown by Prof. Frank Rijsberman, Director, Program, Google.org (formerly Director General of IWMI). Authors also acknowledge numerous people who directly or indirectly contributed to the successful completion of the project. The paper has not been internally reviewed by U.S. Geological Survey (USGS). Hence the views expressed in the paper are not endorsed by USGS.

References

Amthor, J.S., M.o.E.W. Group, 1998. Terrestrial Ecosystem Responses to Global Change: A Research Strategy. Oak Ridge National Laboratory, Oak Ridge, Tennessee.

Bartholomé, E., Belward, A.S., 2005. GLC2000: a new approach to global land cover mapping from earth observation data. International Journal of Remote Sensing 26 (9), 1959–1977.

Biggs, T., Thenkabail, P.S., Krishna, M., Gangadhararao, P., Turral, H., 2006. Vegetation phenology and irrigated area mapping using combined MODIS time-series, ground surveys, and agricultural census data in Krishna River Basin, India. International Journal of Remote Sensing 27, 4245–4266.

CA, 2007. In: David, M. (Ed.), Comprehensive Assessment (CA) of Water Management in Agriculture, Water for Food and Water for Life: A Comprehensive Assessment of Water Management in Agriculture. International Water Management Institute, London: Earthscan and Colombo, pp. 1–645.

Cramer, W.P., Soloman, A.M., 1993. Climatic classification and future global redistribution of agricultural land. Climate Research 3, 97–110.

Defries, R.S., Townshend, J.R.G., 1994. Global land cover: comparison of ground based data sets to classifications with AVHRR data. In: Foody, G.M., Curran, P.J. (Eds.), Environmental Remote Sensing from Regional to Global Scales. Wiley, New York, pp. 84–110.

Defries, R., Hansen, M., Townsend, J.G.R., Sohlberg, R., 1998. Global land cover classifications at 8 km resolution: the use of training data derived from Landsat imagery in decision tree classifiers. International Journal of Remote Sensing 19, 3141–3168.

Defries, R., Hansen, M., Townshend, J., 1995. Global discrimination of land cover types from metrics derived from AVHRR Pathfinder data. Remote Sensing of Environment 54, 209–222.

FAO (Food and Agriculture Organization of the United Nations), 1990. 1989 Production Yearbook. UNFAO, Rome.

FAO (Food and Agriculture Organization of the United Nations), 1991. 1990 Production Yearbook. UNFAO, Rome.

FAO (Food and Agriculture Organization of the United Nations), 2002. World Agriculture Towards 2015/30, Summary Report. Food and Agricultural Organizations of United Nations, Rome, pp. 1–97.

FAOSTAT, 2000. On-Line Statistical Database of the Food and Agricultural Organization of the United Nations. Available online at http://apps.fao.org (accessed 9 February, 2004).

Friedl, M.A., Mciver, D.K., Hodges, J.C.F., Zhang, X.Y., Muchoney, D., Strahler, A.H., Woodcock, C.E., Gopal, S., Schneider, A., Cooper, A., Baccini, A., Gao, F., Schaaf, C., 2002. Global land cover mapping from MODIS: algorithms and early results. Remote Sensing of Environment 83, 287–302.

Goldewijk, K.K., 2001. Estimating global land use change over the past 300 years: the HYDE database. Global Biogeochemical Cycles 15, 417–434.

Grubler, A., 1994. Technology. In: Meyer, W.B., Turner, II, B.L. (Eds.), Changes in Land Use and Land Cover: A Global Perspective. Cambridge University Press, New York, pp. 287–328.

Hansen, M.C., Defries, R.S., Townshend, J.R.G., Sohlberg, R., 2000. Global land cover classification at 1 km spatial resolution using a classification tree approach. International Journal of Remote Sensing 21, 1331–1364.

Homayouni, S., Roux, M., 2003. Material Mapping from Hyperspectral Images using Spectral Matching in Urban Area. In: IEEE Workshop on Advances in Techniques for Analysis of Remotely Sensed Data, Greenbelt, MD, USA, October 2003. IGBP Global Change Report No. 20, International Geosphere–Biosphere Programme, Stockholm, pp. 110–114.

Houghton, R.A., 1999. The annual net flux of carbon to the atmosphere from changes in land use 1850–1990. Tellus 51B, 298–313.

IGBP, 1992. In: Townshend, J.R.G. (Ed.), Improved Global Data for Land Applications.

Kauth, R.J., Thomas, G.S., 1976. The tasseled cap—a graphic description of the spectral-temporal development of agricultural crops as seen by Landsat. In: In Proceedings of the Symposium on Machine Processing of Remotely Sensed Data. West Layfayette, Purdue University, Indiana pp. 4B-41-4B-50.

Lal, R., Pierce, F.J., 1991. Soil Management for Sustainability. World Association of Soil and Water Conservation and the Soil Science Society of America, Ankeny, Iowa.

Lillesand, T.M., Kiefer, R.W., 1987. Remote Sensing and Image Interpretation, second ed. John Wiley and Sons Inc., Toronto.

Loveland, T.R., Reed, B.C., Brown, J.F., Ohlen, D.O., Zhu, J., Yang, L., Merchant, J.W., 2000. Development of a global land cover characteristics database and IGBP DISCover from 1-km AVHRR data. International Journal of Remote Sensing 21, 1303–1330.

Loveland, T.R., Zhu, Z., Ohlen, D.O., Brown, J.F., Reed, B.C., Yang, L., 1999. An analysis of the IGBP global land-cover characterization process. Photogrammetric Engineering and Remote Sensing 65, 1021–1032.

Mackenzie, F.T., Mackenzie, J.A., 1995. Our Changing Earth: An Introduction to Earth System Science and Global Environmental Change. Prentice Hall, New York.

Matthews, E., 1983. Global vegetation and land use: new high resolution databases for climate studies. Journal of climate and applied Meteorology 22, 474–487.

Olson, J.S., 1994. Global Ecosystem Framework: Translation Strategy. USGS EROS Data Center Internal Report, 39 p.

Olson, J.S., Watts, J.A., 1982. Major World Ecosystem Complex Map. Oak Ridge National Laboratory, Oak Ridge, Tennessee.

Preiser, R.F., 2005. Living Within Our Environmental Means: Natural Resources and an Optimum Human Population (http://dieoff.org/page50.htm (accessed 20 December 2007)).

Ramankutty, N., Foley, J.A., 1998. Characterizing patterns of global land use: an analysis of global croplands data. Global Biogeochemical Cycles 12, 667–685.

Ramankutty, N., Foley, J.A., 1999. Estimating historical changes in global land cover: croplands from 1700 to 1992. Global Biogeochemical Cycles 13, 997–1027.

Richards, J.F., 1990. Land transformation. In: Turner, B.L. (Ed.), The Earth as Transformed by Human Action. Cambridge with Clark University, New York.

Rockstrom, J., Barron, J., Fox, P., 2003. Water productivity in rain-fed agriculture: challenges and opportunity for smallholder farmers in drought-prone tropical agroecosystems. In: Kijne, J.W., Barker, R., Molden, D. (Eds.), Water Productivity in Agriculture: Limits and Opportunities for Improvement. CAB International, pp. 145–162.

Siebert, S., Hoogeveen, J., Frenken, K., 2006. Irrigation in Africa, Europe, and Latin America, Update of the Digital Global Map of Irrigation Areas to Version 4. Frankfurt Hydrology Paper 05. FAO, University of Frankfurt (main) and Rome, Germany & Italy.

Thenkabail, P.S., Biradar, C.M., Noojipady, P., Cai, X.L., Dheeravath, V., Li, Y.J., Velpuri, M., Gumma, M., Pandey, S., 2007a. Sub-pixel irrigated area calculation methods. Sensors Journal 7, 2519–2538.

Thenkabail, P.S., Gangadhararao, P., Biggs, T., Krishna, M., Turral, H., 2007b. Spectral matching techniques to determine historical land use/land cover (LULC) and irrigated areas using time-series AVHRR pathfinder datasets in the Krishna River Basin, India. Photogrammetric Engineering and Remote Sensing 73, 1029–1040.

Thenkabail, P.S., Biradar, C.M., Turral, H., Noojipady, P., Li, Y.J., Vithanage, J., Dheeravath, V., Velpuri, M., Schull M., Cai, X.L., Dutta, R., 2006. An Irrigated Area Map of the World (1999) derived from Remote Sensing. Research Report No. 105. International Water Management Institute, Colombo, 74 p.

Thenkabail, P.S., Biradar C.M., Noojipady, P., Dheeravath, V., Li, Y.J., Velpuri, M., Gumma, M., Reddy, G.P.O., Turral, H., Cai, X. L., Vithanage, J., Schull, M., Dutta, R., 2008. Global Irrigated Area Map (GIAM) for the End of the Last Millennium Derived from Remote Sensing. International Journal of Remote Sensing, in press.

Thomas, D.S.G., Middleton, N.J., 1993. Salinization: new perspectives on a major desertification issue. Journal of Arid Environments 24, 95–105.

Tilman, D., Fargione, J., Wolff, B., D'Antonio, C., Dobson, A., Howarth, R., Schindler, D., Schlesinger, W.H., Simberloff, D., Swackhamer, D., 2001. Forecasting agriculturally driven global environmental change. Science 292, 281–284.

Warnant, P., Francois, L., Strivay, D., Gerard, J.C., 1994. Caraib—a global model of terrestrial biological productivity. Global Biogeochemical Cycles 8, 255–270.

Wilson, M.F., Henderson-Sellers, A., 1985. A global archive of land cover and soils data for use in general circulation models. Journal of Climatology 5, 119–143.

World Resources, 1992–1999. A Guide to the Global Environment, Oxford, 1992. Oxford University Press, New York.

WBGU, 1998. Die Anrechnung biologischer Quellen und Senken im Kyoto-Protokoll: Fortschritt oder Ruckschlag fur den globalen Umweltschutz. Sondergutachten, Bremerhaven, Germany.

Wood, S., Sebastian, K., Scherr, S.J., 2000. Pilot Analysis of Global Ecosystems: Agroecosystems. International Food Policy Research Institute (IFPRI) and World Resources Institute (WRI), Washington, DC.

Worldwatch Institute, 2001. Worldwatch Institute, Vital Signs. W.W. Norton and Company, New York.

WRI, 2000. World Resources Institute, World Resources 2000–2001: People and Ecosystems. World Resources Institute, Washington, DC.

WRI, 2003. World Resources Institute, Earth Trends: The Environmental Information Portal. World Resources Institute.

Xiao, X., Melillo, J.M., Kicklighter, D.W., Mcguire, A.D., Tian, H., Pan, Y., Vorosmarty, C.J., Yang, Z., 1997. Transient Climate Change and Potential Croplands of the World in the 21st Century, Joint Program on the Science and Policy of Global Change, Report No. 18, Massachusetts Institute of Technology, Massachusetts.